EUROPEAN FUSION DEVELOPMENT AGREEMENT

EFDA–JET–PR(07)11

I.T. Chapman, T.C. Hender, D.F. Howell, S.K. Erents, M.P. Gryaznevich,
E de la Luna, A. Savchkov, R. Scannell, S. Shibaev, M.F. Stamp,
the MAST team and JET EFDA contributors

Perturbation of Tokamak Magnetic Surfaces by Applied Toroidally Asymmetric Magnetic Fields

Perturbation of Tokamak Magnetic Surfaces by Applied Toroidally Asymmetric Magnetic Fields

I.T. Chapman[1], T.C. Hender[1], D.F. Howell[1], S.K. Erents[1], M.P. Gryaznevich[1], E de la Luna[2], A. Savchkov[3], R. Scannell[4], S. Shibaev[1], M.F. Stamp[1], the MAST team and JET EFDA contributors*

[1]EURATOM-UKAEA Fusion Association, Culham Science Centre, OX14 3DB, Abingdon, OXON, UK
[2]Forschungszentrum Jülich GmbH, Association EURATOM-FZ Jülich, Institut für Plasmaphysik, Trilateral Euregio Cluster, D-52425 Jülich, Germany
[3]Department of Electrical &Electronic Engineering, University College Cork, Association EURATOM-DCU, Ireland
** See annex of M.L. Watkins et al, "Overview of JET Results ", (Proc. 21st IAEA Fusion Energy Conference, Chengdu, China (2006)).*

Preprint of Paper to be submitted for publication in
Nuclear Fusion Letter

ABSTRACT.
The effects of applied 3-dimensional magnetic error fields on magnetic surfaces are measured in both the Joint European Torus (JET) and the Mega Ampere Spherical Tokamak (MAST). Static perturbation fields with various amplitudes have been applied in both devices using non-axisymmetric coils producing a dominantly n = 1 magnetic field to systematically perturb the plasma flux surfaces. The displacement of the plasma boundary is found to increase linearly with the strength of the applied field, and agrees well with predictive modelling which superimposes vacuum non-axisymmetric fields on a 2d equilibrium.

INTRODUCTION

Imperfections in the construction and alignment of tokamak magnetic field coils inevitably lead to non-axisymmetric error fields. These error fields have been observed to have detrimental effects on the plasmas in many tokamaks, including JET [1] and MAST [2]. For instance, the error fields can induce locked tearing modes with low toroidal and poloidal mode numbers. At low levels of error field, plasma rotation can suppress these tearing modes [3, 4], but as the error field increases a threshold will be reached at which point a non-rotating (or locked) mode grows, quenches the plasma rotation and often terminates the discharge [3, 5]. This effect, known as error field penetration, occurs for error fields of the order of the anticipated intrinsic error field resulting from alignment inaccuracies. As such, JET and MAST (as well as other tokamaks) have installed Error Field Correction Coils (EFCCs) in order to ameliorate the intrinsic error field by applying an opposing non-axisymmetric magnetic field. As well as counter-acting the intrinsic error fields, the EFCCs have been employed as a method for mitigating Edge Localised Modes (ELMs) [6–8] by ergodising the flux surfaces at the plasma edge.

When the EFCCs are applied, it is important to know how the plasma responds to the non-axisymmetric fields for various reasons, including plasma position control, equilibrium reconstruction and diagnostic measurements, as well as for basic physics understanding. Previous experiments on DIII-D [9] to measure the perturbation of the flux surfaces due to applied error fields suggested that the plasma experienced a “balloon-like” response, whereby as the error field was increased, the perturbation increased more rapidly than was predicted to occur due to the applied field alone. In the DIII-D experiments a slowly-rotating error field was applied, and the non-linear scaling of the perturbation with respect to the applied field led Lao et al [9] to suggest that the plasma contribution to the response was important. In this paper, static error fields are applied in both JET and MAST, and the flux surface displacement is found to increase linearly with respect to the error field amplitude.

The JET error field correction system consists of four coils arranged symmetrically around the outside of the vacuum vessel, with each coil spanning 70%æ toroidally [10]. Each coil has 16 turns and carries a maximum of 3kA in a single turn. The coils are located in Octants 1, 3, 5 and 7 of the vessel, with toroidally opposite coils having oppositely directed currents to produce an odd-n spectrum. Fourier analysis of the normal component of the applied field in straight field line coordinates (θ, ϕ)

$$B_{m,n} = \frac{\alpha_{mn}}{2\pi^2} \int_0^{2\pi} \int_0^{2\pi} B_\perp (\theta, \phi) \exp i(m\theta + n\phi)\, d\theta d\phi \qquad (1)$$

where $B_\perp$ is the applied field normal to the $q = 2$ surface and mn is a normalisation factor such that $\alpha_{00} = 0.5$ and $mn = 1$ for all other m and n. The Fourier spectrum of the component of the applied magnetic field normal to the $q = 2$ surface when one pair of coils are powered is shown in Figure 1. It can be seen that the dominant resonant component of the applied field is the $n = 1$, $m = 1$ harmonic. There are also four ex-vessel coils on MAST, each spanning 83^o toroidally and containing three turns, each capable of carrying 5kA. The two pairs of coils are known as 'EFC-A' (located in sectors 5 and 11 (of 12)) and 'EFC-B' (located in sectors 2 and 8) and are fed by independent power supplies, allowing an arbitrary toroidal phase for the applied field. In these experiments the EFCCs are arranged in two pairs, with opposite coils wired in series to produce a dominantly $n = 1$ magnetic field. The coils are supplied with direct current yielding a static perturbation field. Figure 2 shows the Fourier spectrum of the radial applied field normal to the $q = 2$ surface when the EFC-A coils are applied. For a MAST equilibrium the dominant resonant component of the applied field is the $n = 1$, $m = 1$ harmonic.

In order to measure the perturbation of edge flux surfaces by the applied error fields, the amplitude and phase of the static field was varied in both tokamaks, and measurements of edge density and temperature were made. In JET, the pertinent diagnostics used were the reciprocating probe, which measured the electron density at $Z = 1.56$m in Octant 5, and the Electron Cyclotron Emission heterodyne radiometer (ECE), which measured the electron temperature with a spatial resolution of approximately 5cm along a horizontal chord at $Z = 0.133$m in Octant 7. In MAST, the reciprocating probe measured the electron temperature and density at the equatorial plane in Sector 1, the edge Thomson scattering system measured the electron density and temperature along the midplane of Sector 11 and the high speed Photron camera sees the whole plasma cross-section looking towards Sector 5. The experiments on bothmachines were performed in steady state L-mode plasmas.

In the JET experiments the following set of plasma parameters was used: $I_p = 1.9$MA, $B_T = 2$T, $n_e \approx 1.7 \times 10^{19} m^{-3}$, Ohmic plasmas with $\beta_p = 2\mu 0p/B_P^2 = 0.35$ and $q_{95} = 3.35$, where B_P is the poloidal magnetic field. Static error fields were applied substantially below the locked mode threshold [11], first with positive current supplied to the EFCCs, then with negative current. Measurements were taken with the reciprocating probe and the ECE for each phase and amplitude of the applied error field. Figure 3 shows ECE measurement of the edge electron temperature for two identical discharges with opposite phase of applied error field from the (3,7) coils. There is a distinct shift of the edge plasma outwards when a field is applied at 270^o (ie positive current is applied in the (3,7) EFCCs), and inwards when the applied field is in 90^o phasing. As the amplitude of the applied field is increased, the displacement of the plasma edge increases monotonically. It is important to note that the edge pedestal density is not perfectly stationary over this period (varies by ~15%), and the density evolution itself can lead to a radial perturbation of the isotherms. However, the density

profile evolves in the same way in the two shots, yet the temperature profiles shift in opposite directions, suggesting that the applied field is affecting the plasma edge. A similar displacement of the edge flux surfaces is exhibited by the reciprocating probe measurements. Figure 4 illustrates the electron density when different phases of error field are applied to the same discharge using the (1,5) coils. It is evident once again that the applied field causes a shift of the plasma edge of approximately 10mm. It should be noted that there is a position and shape controller on JET which applies axisymmetric fields to the plasma in order to restore the plasma column to the radial location of its sensors, which are located in Octants 3 and 7. This may result in an outward shift as the controller moves the plasma vertically or shrinks/expands the plasma column. Here, the change in the current passing through the poloidal field coils when the EFCCs are applied could only account for a shift at the location of the edge diagnostics which was an order of magnitude smaller than that observed. In contrast, the change in the current in the poloidal field coils when the error fields were applied in Reference [7] arose partially due to a larger“ and was significantly greater than in these experiments.

The TORFLD code [12], which follows field lines in general toroidal geometry using the arc length along the field line as the independent variable of integration, has been used to model the perturbation due to the EFCCs. An equilibrium solution of the static Grad-Shafranov equation is calculated using the EFIT code [13] and then a vacuum field of the perturbation is applied using TORFLD in order to simulate the flux surface displacement. Since the toroidal and radial locations of the diagnostics are known, it is possible to predict what the displacement will be for a given applied error field. Figure 5 shows the perturbation predicted by TORFLD compared to the experimental observations. The modelling suggests that the perturbation increases linearly as the amplitude of the error field increases, and this trend is exhibited in the JET results too. The modelled perturbation of the flux surfaces suggests that the dominant edge distortion is caused by an n/m = 1/1 mode, as shown in Figure 6, where the perturbation is seen to have a periodicity of one in both the poloidal and toroidal directions. Figure 6 shows Poincare puncture plots, one sliced through the midplane when $z = 0$ showing the shift in R at various toroidal angles, ϕ, and the second at constant ϕ showing the perturbation arising from the applied fields in r for varying poloidal angle, θ. This would be consistent with a non-resonant response, perhaps explaining why modelling by superimposing a vaccum field gives good qualitative agreement with the shifts exhibited experimentally. In order to account for any displacement caused by the shape controller, the field generated by the change in the current passing through the poloidal field coils is included in the modelling. The effect of this poloidal field is to expand or shrink the plasma column on both the inboard and outboard side, in accordance with Reference [7]. However, in these experiments the perturbation resulting from the shape controller is found to be significantly smaller than the shift due to the applied error field.

In MAST, the following set of experimental parameters was used: $I_p = 0.7$MA, $B_T = 0.4$T, $n_e \approx 3.0\times10^{19}\,m^{-3}$, Ohmic plasmas with $\beta_p = 0.2$ and $q_{95} = 5.0$. Again, static error fields below the locked mode threshold [2] were applied in each pair of coils with different phasing and amplitude and with

corrections for the intrinsic error field included. The radial position controller was disabled before the EFCCs were applied. The perturbation measured by the edge Thomson scattering is illustrated in Figure 7, showing a displacement of approximately 1cm when the EFC-A coils are applied. Figure 8 shows the absolute difference between two discharges seen by the high speed Photron camera when the EFC-B coils are applied. The displacement is measured by finding two frames with steady plasma edges and nominal filamentary activity and subtracting the images to find the difference in pixel space. This is then mapped to real space by using images of vessel components of known dimensions. Finally, the lens distortion of the image edge is corrected and the perturbation is ascertained to be approximately 2cm in Figure 8. Normally, the images would be Abel inverted to calculate the plasma shift in pixel space, but this process assumes axisymmetry, which is broken by the application of error fields. We assume that since the shift is a small perturbation to the plasma length scale, then the conversion factor from pixel to real space will be approximately the same at the plasma edge and the centre column. The perturbation due to the applied error fields is found to agree well with TORFLD modelling, in good accordance with the JET data. Figure 9 shows the modelling prediction for the edge perturbation compared with the experimental measurements from the high speed cameras.

The DIII-D experiments [9] did exhibit a linear response at smaller applied fields, and only witnessed a “ballooning” of the difference between the measured plasma edge and the magnetic reconstruction assuming toroidal symmetry when the applied field approached the locked mode threshold. Since care has been taken not to trigger locked modes in the studies in this paper, the applied fields may be insufficient to cause a displacement of the plasma edge which does not scale linearly with the applied field.

Experiments have been undertaken on a conventional aspect ratio tokamak (JET) and a spherical tokamak (MAST) to quantitatively assess the perturbation of the edge flux surfaces when error fields are applied. The plasma in both devices has been perturbed by applied fields of increasing amplitude and different phasing. The edge plasma response was measured by using various different diagnostics and compared with vacuum field modelling. It has been shown that the perturbation of the plasma edge increases linearly with the amplitude of the applied error field, in good agreement with the predictions of a field line following model.

ACKNOWLEDGMENTS

Thanks to Dr HR Koslowski and Dr Y Liang for numerous useful discussions. This work was funded jointly by the United Kingdom Engineering and Physical Sciences Research Council and by the European Communities under the contract of Association between EURATOM and UKAEA. The views and opinions expressed herein do not necessarily reflect those of the European Commission. This work was carried out within the framework of the European Fusion Development Agreement.

REFERENCES

[1]. Buttery R.J. et al 2000 Nucl Fusion **40** 807

[2]. Howell D.F., Hender T.C. and Cunningham G 2006 sub Nucl. Fusion

[3]. Fitzpatrick R. and Hender T.C. 1994 Phys. Plasmas **1** 3337

[4]. Koslowski H.R. et al 2006 Nucl. Fusion **46** L1

[5]. Hender T.C. et al 1992 Nucl. Fusion **32** 2091

[6]. Evans T.E. et al 2005 Journal of Nucl. Materials **337** 691

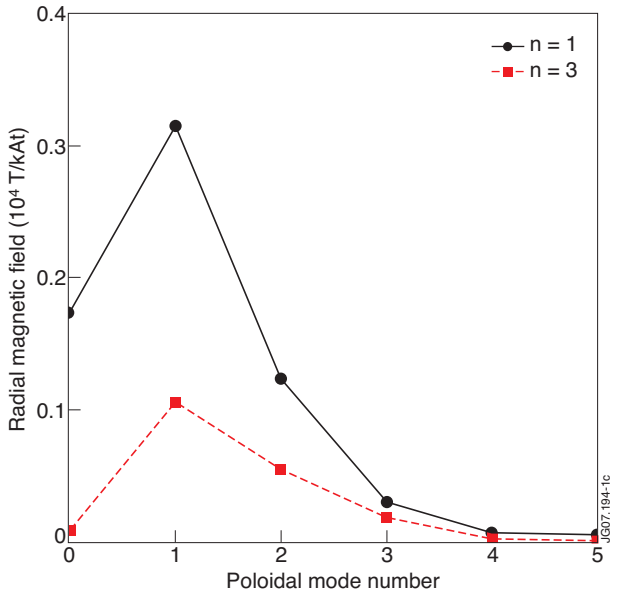

Figure 1: The applied magnetic field spectrum from the JET (3,7) error field correction coils at q = 2 for an equilibrium with I_p = 1.9MA, B_T = 2T, $n_e = 1.7\times10^{19}m^{-3}$, κ = 1.65 and δ = 0.3. The dominant resonant component of the applied field is the n = 1, m = 1 harmonic.

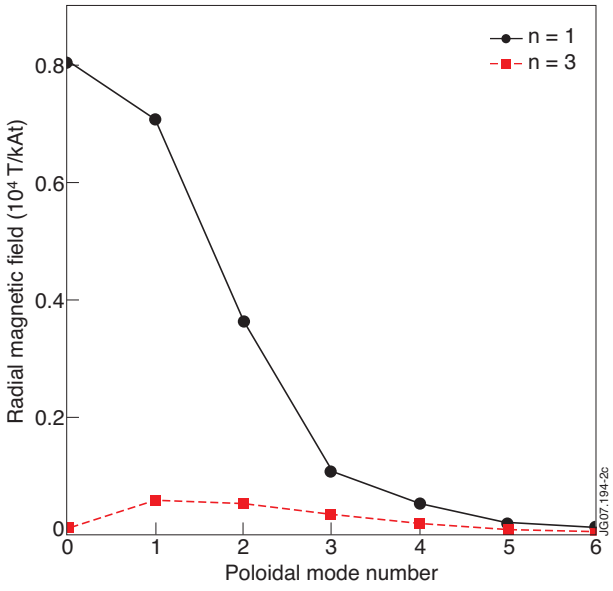

Figure 2: The applied magnetic field spectrum from the MAST EFC-A error field correction coils at q = 2 for an equilibrium with I_p = 700kA, B_T = 0.4T, $n_e = 2.9\times10^{19}m^{-3}$, κ = 1.9 and δ = 0.4. The dominant resonant component of the applied field is the n = 1, m = 1 harmonic.

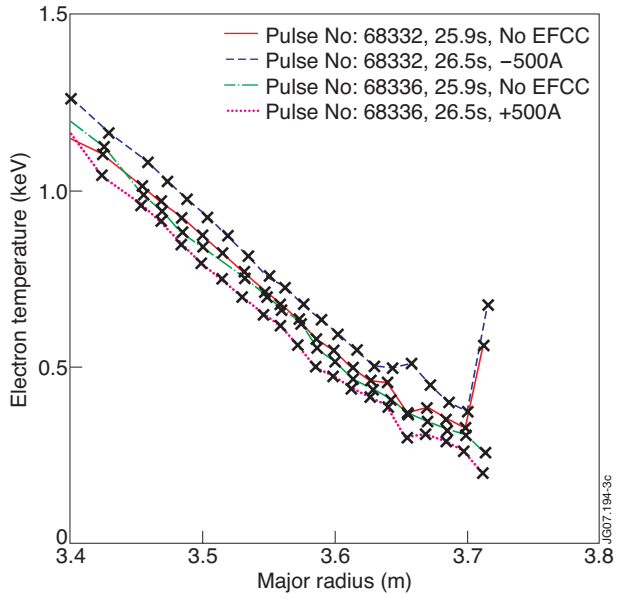

Figure 3: The Electron Cyclotron Emission Heterodyne Radiometer measurement of the edge plasma electron temperature as a function of radius for JET Pulse No's: 68332 (−500A) and 68336 (+500A). A displacement of 12mm results from the applied error field.

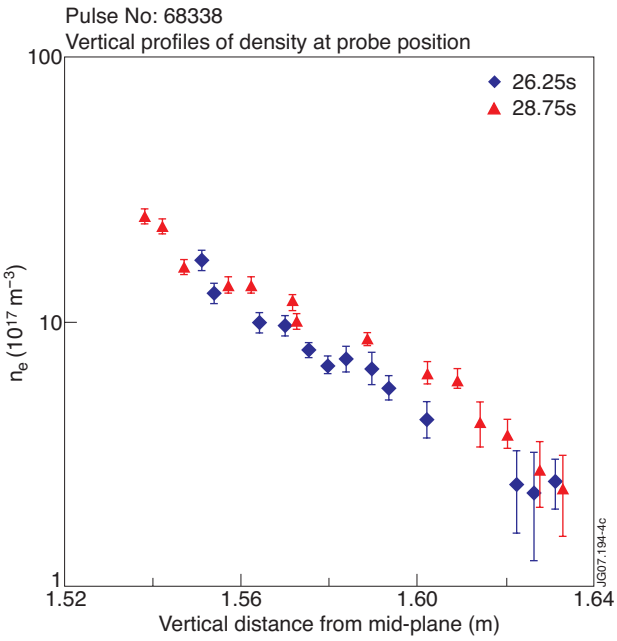

Figure 4: The reciprocating probe measurement of the electron density as a function of the vertical distance of the probe from the mid-plane for JET Pulse No: 68338. The edge flux surfaces are observed to move by approximately 10mm between the +500A (68.75s) and −500A (66.25s) phase in the (1,5) EFCCs.

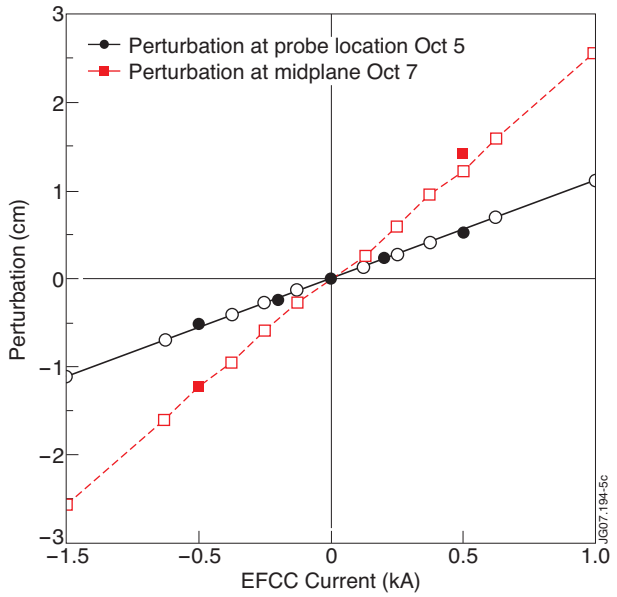

Figure 5: The predicted edge perturbation (lines and open symbols) in Octant 5 (Reciprocating Probe - circles) when the (1,5) coils are applied and Octant 7 (ECE - squares) when the (3,7) coils are applied in JET agrees well with experimental data (filled symbols) and exhibits a linear response to the applied error field.

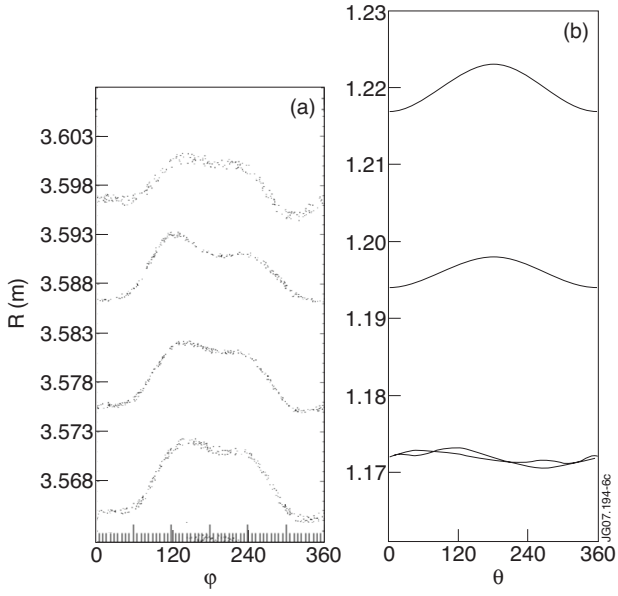

Figure 6: Poincare plots showing the periodicity of the shift caused by the applied error fields in the toroidal and poloidal directions. Figure (a) shows the field line variation in major radius, R with respect to the toroidal angle, ϕ at the midplane, $z = 0$. Figure (b) shows the field line variation in minor radius, r with respect to poloidal angle, θ, at constant toroidal location, $\phi = 0$.

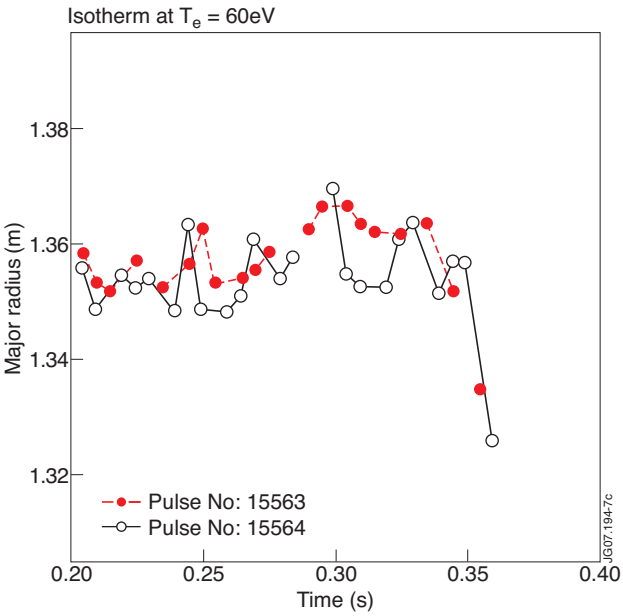

Figure 7: 60eV isotherms measured by the Edge Thomson Scattering show approximately 1cm perturbation in the edge plasma between MAST Pulse No's: 15563 (−2.3kA) and 15564(+500A).

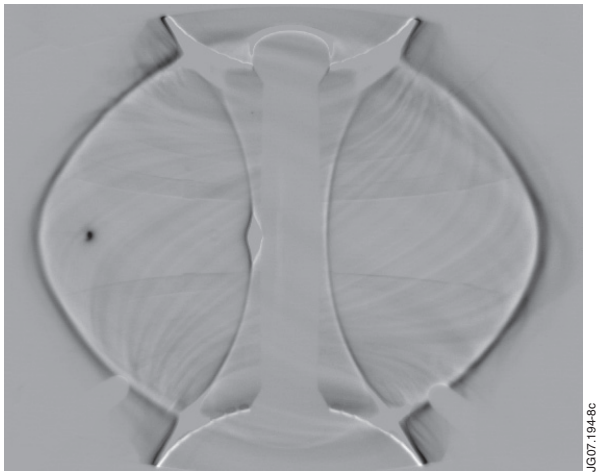

Figure 8: The subtracted image from the Photron high speed camera indicates a perturbation (black outline shows absolute difference) of approximately 2cm between MAST discharge 15572 (+1.2kA) and 15573 (-1.2kA).

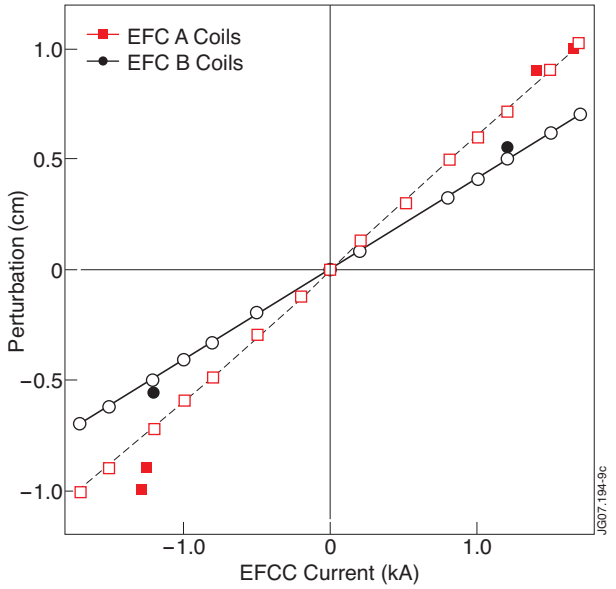

Figure 9: The predicted edge perturbation (lines and open symbols) in MAST using each pair of coils agrees well with experimental data (filled symbols) and exhibits a linear response to the applied error field.